Available online at www.sciencedirect.com
SCIENCE DIRECT®
Catalysis Today 85 (2003) 145–152
CATALYSIS TODAY
www.elsevier.com/locate/cattod

Electronic and structural properties of $Sn_xTi_{1-x}O_2$ solid solutions: a periodic DFT study

Fabrício R. Sensato [a,*], Rogério Custodio [a], Elson Longo [b], Armando Beltrán [c,*], Juan Andrés [c]

[a] *Instituto de Química, Universidade Estadual de Campinas, CP 6154, 13083-970 Campinas, SP, Brazil*
[b] *Departamento de Química, Universidade Federal de São Carlos, CP 676, 13565-905 São Carlos, SP, Brazil*
[c] *Departamento de Ciències Experimentals, Universitat Jaume I, Apartat 224, 12080 Castelló, Spain*

Received 27 February 2003; received in revised form 31 May 2003; accepted 9 June 2003

Abstract

The structural and electronic properties of selected compositions of $Sn_xTi_{1-x}O_2$ solid solutions ($x = 0$, 1/24, 1/16, 1/12, 1/8, 1/6, 1/4, 1/2, 3/4, 5/6, 7/8, 11/12, 15/16, 23/24 and 1) were investigated by means of periodic density functional theory (DFT) calculations at B3LYP level. The calculations show that the corresponding lattice parameters vary non-linearly with composition, supporting positive deviations from Vegard's law in the $Sn_xTi_{1-x}O_2$ system. Our results also account for the fact that chemical decomposition in $Sn_xTi_{1-x}O_2$ system is dominated by composition fluctuations along [0 0 1] direction. A nearly continuous evolution of the direct band gap and the Fermi level with the growing value of x is predicted. Ti 3d states dominate the lower portion of the conduction band of $Sn_xTi_{1-x}O_2$ solid solutions. Sn substitution for Ti in TiO_2 increases the oxidation–reduction potential of the oxide as well as it renders the lowest energy transition to be indirect. These two effects can be the key factors controlling the rate for the photogenerated electron–hole recombination. These theoretical results are capable to explain the enhancement of photoactivity in $Sn_xTi_{1-x}O_2$ solid solutions.

Keywords: Oxidation–reduction potential; Electron–hole recombination; Fermi level; SnO_2-TiO_2; Periodic DFT calculation; Photocatalysis

1. Introduction

The adsorption of gaseous molecules on the surface of some simple semiconductor oxides, among them SnO_2 and TiO_2, is known to change the conductivity of the material affording the use of this feature for purpose of gas detection. Due to their chemical stability and their intrinsic mechanism of detection, SnO_2 and TiO_2 are employed in a wide range of thermodynamic conditions. Owing to its high sensitivity to the reducing atmosphere, SnO_2 is the most used oxide as active component of sensor devices. Relatively low thermodynamic stability manifested by its high equilibrium oxygen pressure ($SnO_2 \leftrightarrow SnO + (1/2)O_2$) is responsible for the degradation of its electrical properties upon prolonged thermal treatment in reducing gas atmosphere [1]. On the other hand, TiO_2 exhibits much lower equilibrium pressure of oxygen than that of SnO_2, and consequently, major resistance to the reducing atmosphere. As far as the mechanism of detection is concerned, SnO_2 and TiO_2 present different behavior. Surface and bulk interactions control the gas sensing mechanism of SnO_2- and TiO_2-based devices, respectively. This fact has profound implications

* Corresponding authors.
E-mail addresses: sensato@iqm.unicamp.br (F.R. Sensato), beltran@exp.uji.es (A. Beltrán).

0920-5861/$ – see front matter © 2003 Elsevier B.V. All rights reserved.
doi:10.1016/S0920-5861(03)00382-1

in the applicability of these oxides as ultimate component in gas sensor devices, since surface interactions restrict their use at moderate temperatures (300–400 °C), while bulk interaction, in which the bulk TiO_2 diffusion of defects determines the sensor response, restricts the operating system to temperatures on the order of 1000–1200 °C (due to extremely high TiO_2's resistivity) [2].

$Sn_xTi_{1-x}O_2$ system has proven to be a good candidate for gas sensor [1,3–6] and low-voltage varistor [7] application. For example, small additions of SnO_2 to TiO_2 lattice allow the operating temperature for hydrogen sensor to be lowered to about 500 °C [3]. It has also been shown that the response of SnO_2 sensors containing small additions of Ti is comparable with that of undoped SnO_2, however the long-term stability is improved [4]. In addition, the use of $Sn_xTi_{1-x}O_2$ solid solution in environmental catalysis has also been examined because of its photocatalytic activity as it exhibits high quantum yield. It has been shown that small Sn substitution for Ti in rutile TiO_2 increases the photoactivity of the rutile by 15 times for the oxidation of acetone [8]. Addition of Sn into TiO_2, endows the catalyst with major photoactivity to decompose methyl orange which is an organic compound model that exhibits good resistance to light degradation [9]. Yet, $Pt/Sn_xTi_{1-x}O_2$ (at higher TiO_2 contents) appears to be a good catalyst for CO oxidation [10].

Due to their similar structure and close lattice parameters (tetragonal rutile (Fig. 1), lattice constants SnO_2, $a = 4.738$ Å and $c = 3.188$ Å, and TiO_2, $a = 4.593$ Å and $c = 2.959$ Å), it is possible to obtain solid solutions $Sn_xTi_{1-x}O_2$ from SnO_2 and TiO_2 under certain processing conditions. Indeed, the phase diagram for SnO_2–TiO_2 binary composition predicts an immiscibility dome, where favorable conditions are created for spinodal or chemical decomposition (unmixing; formation of the modulated phase composed of TiO_2-rich and SnO_2-rich plates) [11–13]. However, even in this region, which is function of the temperature, $Sn_xTi_{1-x}O_2$ solid solutions can be obtained, since the conditions of growth are out of equilibrium [2]. It is expected that the $Sn_xTi_{1-x}O_2$ system could reconcile the best features of its pure components, for instance, remarkable sensing properties of SnO_2 for reducing gases, combined with the good chemical stability of TiO_2 at high temperatures. The knowledge of the bulk electronic structure of this mixed oxide would aid in the design of gas sensing devices and catalysts exhibiting unique features. Therefore, the structural and electronic properties of $Sn_xTi_{1-x}O_2$ solid solutions have been subjected to extensive experimental [1,3–6,8,12–19] and recent theoretical [20] studies. A detailed understanding of the electronic structure of $Sn_xTi_{1-x}O_2$ solid solution, however, lags behind these achievements.

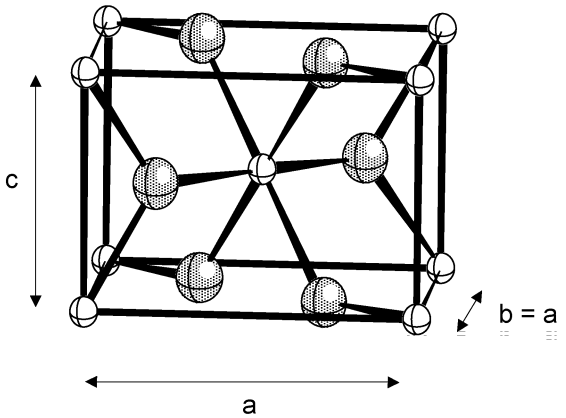

Fig. 1. Primitive unit cell of the bulk rutile structure, space group $P4_2mnm$. Small white balls correspond to titanium (or tin) atoms, and big light gray balls to the oxygen atoms. There are two units of TiO_2 (or SnO_2) in the unit cell.

Over the last years, first-principles calculations have been recognized as an outstanding tool so as to elucidate the electronic structure of crystalline materials [21–27]. Reliable description of the electronic structure of rutile-type compounds has been achieved by means of density functional theory (DFT) periodic calculations. Although the electronic properties of bulk and surfaces of the end-members oxides TiO_2 [28–32] and SnO_2 [33–38] have been extensively studied in the literature, no periodic first-principles study has been done for the $Sn_xTi_{1-x}O_2$ system. Here we report a DFT periodic study on selected compositions of $Sn_xTi_{1-x}O_2$ solid solution. Results are discussed in terms of density of states (DOS) and band structure.

2. Computing method and model system

Calculations were performed with the Crystal'98 program package [39]. Becke's three-parameter hybrid non-local exchange functional [40] combined

with the Lee–Yang–Parr gradient-corrected correlation functional [41], B3LYP, has been used. This hybrid functional has been shown to reproduce observed geometrical parameters and band gaps reliably in a wide variety of materials. DFT/B3LYP results are at least as good as those obtained with more sophisticated correlated calculations or perturbation theories [42,43]. Furthermore, DFT/B3LYP approach was also employed in our recent studies on the electronic and structural properties of the bulk and surfaces of SnO_2 [37] and TiO_2 (anatase) [44] systems. Sn, Ti and O centers have been described in the scheme [DB]-21G, [DB]-21G and [DB]-31G, respectively, where [DB] stands for the Durand–Barthelat's non-relativistic large effective core potential [45]. The definition of core and valence electrons is as follows: Sn = $[Kr]5s^25p^2$, Ti = $[Ar]4s^23d^2$ and O = $[He]2s^22p^4$. The corresponding exponents and coefficients for the valence double-zeta basis set representing the Sn and O centers have already been reported in our previous study [34], while the valence basis set for Ti has been taken from [46]. The band structure was obtained at 80 $\vec{k}$ points along the appropriate high-symmetry paths of de Brillouin zone for a tetragonal primitive system.

We have performed electronic structure calculations for $Sn_xTi_{1-x}O_2$ solid solution at $x = 0$, 1/24, 1/16, 1/12, 1/8, 1/6, 1/4, 1/2, 3/4, 5/6, 7/8, 11/12, 15/16, 23/24 and 1. The calculations for end-members oxides TiO_2 and SnO_2 are performed using the conventional unit cell as the building unit. Models representing $Sn_xTi_{1-x}O_2$ solid solutions where $0 < x < 1$ are built within the supercell approach. A supercell is obtained by defining the new unit cell vectors as linear combinations of the primitive unit vectors. The point symmetry is defined by the number of symmetry operators in the new cell. The new translation vectors (a', b', c') are defined in terms of the old vectors (a, b, c). The symmetry is automatically reduced to the point symmetry operators without transitional components. Atoms that are related by symmetry in the unit cell are considered inequivalent in a supercell. Our supercell models are made as follows: at $x = 1/24$ and 23/24 we use a $2\times2\times3$ supercell ($a' = 2\times a$, $b' = 2\times b$, $c' = 3\times c$), at $x = 1/16$ and 15/16 a $2\times2\times2$ supercell ($a' = 2\times a$, $b' = 2\times b$, $c' = 2\times c$), at $x = 1/12$ and 11/12 a $1\times2\times3$ supercell ($a' = a$, $b' = 2\times b$, $c' = 3\times c$), at $x = 1/8$ and 7/8 a $1\times2\times2$ supercell ($a' = a$, $b' = 2\times b$, $c' = 2\times c$), at $x = 1/6$ and 5/6 a $1\times1\times3$ supercell ($a' = a$, $b' = b$, $c' = 3\times c$), at $x = 1/4$ and 3/4 a $1\times1\times2$ supercell ($a' = a$, $b' = b$, $c' = 2\times c$), and at $x = 1/2$ a $1\times1\times1$ supercell ($a' = a$, $b' = b$, $c' = c$). The total energy of each studied model has been minimized with respect to the tetragonal lattice constants a and c and the internal parameter u. Different optimization algorithms have been tested to yield similar results, and the less computationally demanding Nelder–Mead [47] method has been finally used. Optimizations have been carried out until the convergence in the energy achieved 10^{-5} a.u. The XCrysDen program was used to draw the band structure diagram [48].

3. Results and discussion

3.1. Structural properties

In Fig. 2, the calculated values of the lattice parameters c and a, are plotted as a function of x for $Sn_xTi_{1-x}O_2$. The axial ratio c/a and the unit-cell volume $V = a^2c$ are also presented. A comparison of these results with experimental data reported by Hirata et al. [18] shows good agreement. It is evident that the lattice parameters and cell volume of the solid solutions increase with x indicating the lattice expansion. However, the magnitude of the corresponding structural parameters a and c do not vary linearly with x. Therefore, some deviation from Vegard's law is found. Hirata et al. [18] and Park et al. [19], in contrast with the interpretation done by some authors [11,15], also reported positive deviations from Vegard's law in the $Sn_xTi_{1-x}O_2$ system, that is, the lattice parameters are greater than those obtained just from a linear interpolation from the endpoint binary oxides TiO_2 and SnO_2. Thus, our results indicate that the deviation from Vegard's law in the $Sn_xTi_{1-x}O_2$ solid solution is not a consequence of the spinodal decomposition. Deviation from Vegard's law is, however, frequently accompanied by phase separation caused by spinodal decomposition. This behavior can be rationalized by an analysis of Fig. 2. As a rule, the composition should fluctuate in the direction which minimizes the elastic strain while maintaining coherency. In particular, it can be observed from Fig. 2 that the c lattice parameter experiences a larger deviation from the linearity than do so the a parameter. Thus, our results suggest that the [0 0 1] coherent

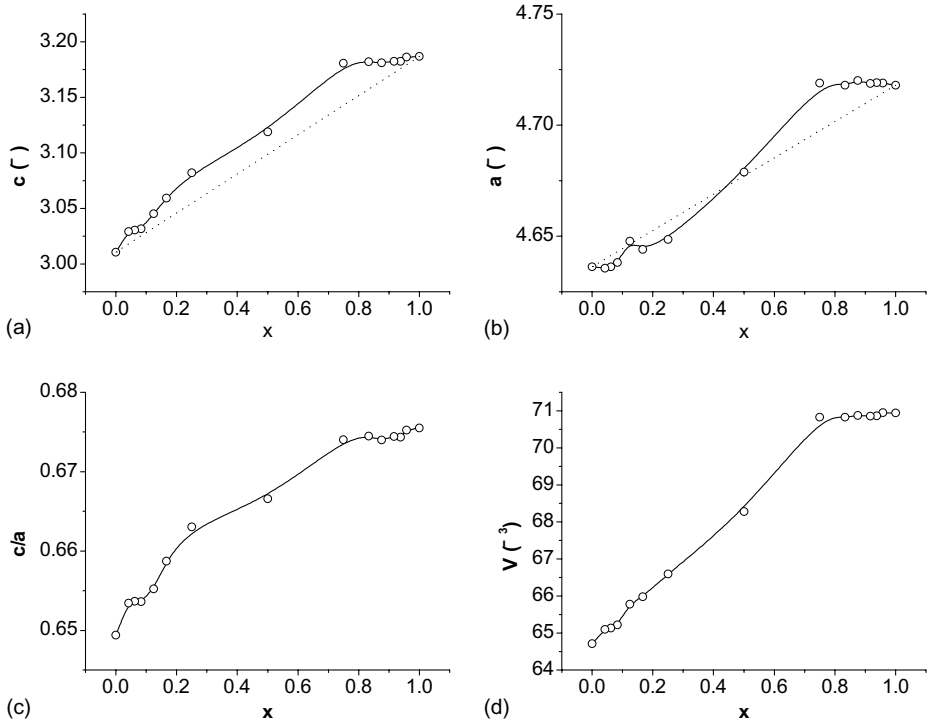

Fig. 2. Calculated lattice parameters: (a) c, (b) a, (c) the axial ratio c/a, and (d) the unit-cell volume (V) as a function of x for $Sn_xTi_{1-x}O_2$ solid solution.

spinodal is then relevant for this system. In fact, it has been shown by experiments that decomposition in the $Sn_xTi_{1-x}O_2$ system is dominated by composition fluctuations along [0 0 1] direction [11,19].

Fig. 2d shows that the unit-cell volume of $Sn_xTi_{1-x}O_2$ increases monotonously with x. This behavior can be explained by the fact that the lattice of the $Sn_xTi_{1-x}O_2$ relax as Sn^{4+} with a larger ionic radius is substituted for Ti^{4+} in TiO_2 [18].

3.2. Electronic structure

In Fig. 3, we display how energies related to the top of the valence band, the bottom of the conduction band, the direct band gap and Fermi level of $Sn_xTi_{1-x}O_2$ solid solutions vary with x. The corresponding Fermi levels were estimated by the equation $E_F = E - E_g/2$, where E is the energy related to the bottom of the conduction band and E_g the band gap. Sn and Ti are isovalent, thus Sn substitution for Ti in rutile TiO_2 or vice versa, does not give rise to extra electrons in the conduction band or holes in the valence band of the material, and therefore, there is no reason for the Fermi level shifting away from its ideal mid-gap position. From an analysis of Fig. 3, it is observed continuous evolution of all these electronic parameters from those of TiO_2, $x = 0$, to those of SnO_2, $x = 1$. For instance, the Fermi level monotonically increases with x, resulting in a separation of 1.1 eV between end members. Still, the direct band gap increases continuously with increasing SnO_2 concentration from about 2.9 eV for TiO_2 to 3.3 eV for SnO_2. In particular, a systematic shift in the fundamental absorption edge with the growing content of SnO_2 in TiO_2 films has been verified by experiment [3].

We have calculated the electronic DOS, i.e. the total number of electronic states per unit energy, for all values x here considered. Since there are no substantial differences in the structure of the corresponding DOS of TiO_2-rich solid solutions ($O < x < 1/2$) and between the SnO_2-rich ones ($1/2 < x < 1$), we present and discuss the total and atom-resolved partial

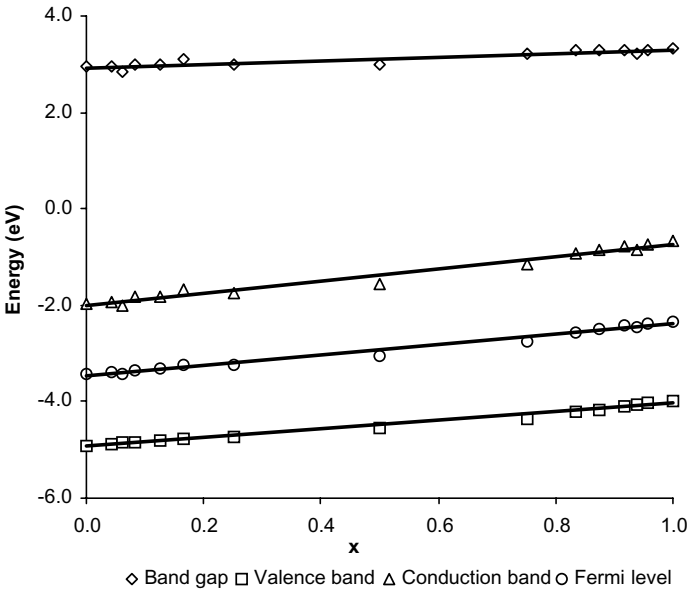

Fig. 3. Energies related to the band gap, the top of the valence band, the bottom of the conduction band and Fermi level of $Sn_xTi_{1-x}O_2$ solid solutions in function of x.

DOS of $Sn_xTi_{1-x}O_2$ at $x = 1/4$ and 3/4. The former is intended to represent the TiO_2-rich solid solutions, while the latter refers to the SnO_2-rich systems.

The total and partial DOS for $Sn_{0.25}Ti_{0.75}O_2$ ($x = 1/4$) is shown in Fig. 4. The zero of the energy was set at the top of the valence band. The upper valence band is made up predominantly of the O 2p components and its width is calculated to be about 8.0 eV. There is also a very limited Ti 3d and Sn 5s contribution in this energy range. The lower valence band region between −20.0 and −17.5 eV, originates essentially from O 2s component. Between these valence bands, there is a wide region, around 9.5 eV, which is devoid of electronic states. The direct band gap for this composition is 3.0 eV. The region above the conduction band edge (comprised between 3.0 and 7.5 eV) is contributed mainly by Ti 3d. Sn 5s and Sn 5p states are mainly located above 8.5 eV.

In Fig. 5, the total and partial DOS for $x = 3/4$ are displayed. Again, the upper valence band is constituted by O 2p states, however its width is of 9.0 eV, which is somewhat larger than that for $x = 1/4$. Again, the Ti 3d states dominate the lower portion of the conduction band of $Sn_xTi_{1-x}O_2$ solid solutions, thus the conduction band is an admixture of extended Sn 5s states and more localized Ti 3d states. The corresponding band gap, E_g, is 3.2 eV.

The exact location of energy levels induced by Ti into the band gap of bulk SnO_2 was determined with the largest $2 \times 2 \times 3$ supercell ($x = 23/24$) in order to minimize defect–defect interactions. The bandwidth of the Ti-induced states was found to be 0.3 eV, while the difference in energy between top of the O 2p valence-band states and the bottom of the Sn 5s conduction-band states increases from the calculated value of 3.3 eV for pure SnO_2 to 3.8 eV for Ti-doped SnO_2. The center of the Ti-induced states is approximately 0.3 eV below the Sn 5s manifold.

3.3. Photocatalytic activity of $Sn_xTi_{1-x}O_2$ solid solutions

In a semiconductor when a photon with energy of $h\nu$ matches or exceeds its band gap energy, E_g, an electron is promoted from the valence band into the conduction band leaving a hole behind. Excited-state conduction-band electrons and valence-band holes can react with electron donors and electron acceptors on the semiconductor surface or recombine and dissipate the input energy as heat. Thus, if suitable electron and

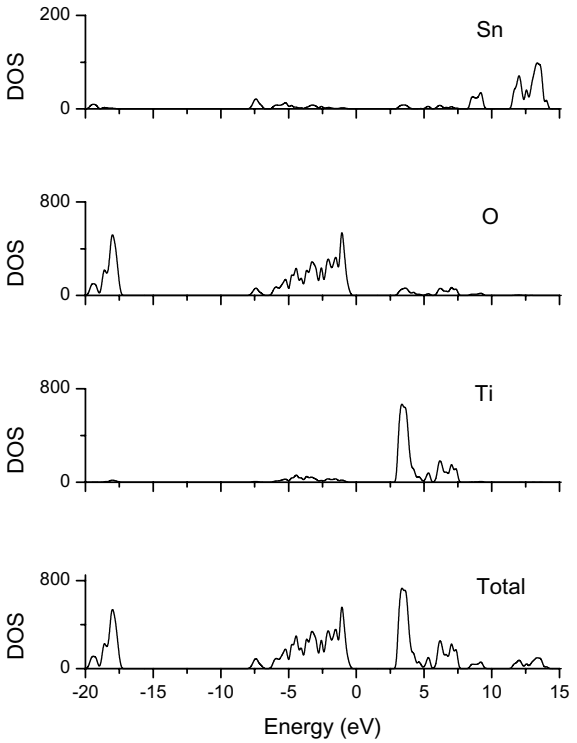

Fig. 4. Total and atom-resolved partial DOS (a.u.) of $Sn_{0.25}Ti_{0.75}O_2$ ($x = 1/4$). The top of the valence band has been taken as energy zero.

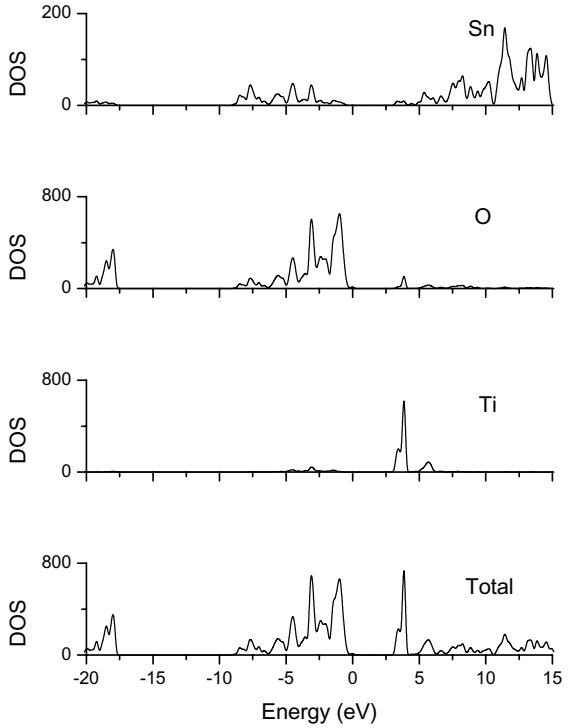

Fig. 5. Total and atom-resolved partial DOS (a.u.) of $Sn_{0.75}Ti_{0.25}O_2$ ($x = 3/4$). The top of the valence band has been taken as energy zero.

hole scavengers are available to trap the electron or hole, recombination is suppressed and the photoactivity of the semiconductor catalyst is enhanced.

Lin et al. found that Sn substitution for Ti in rutile TiO_2 increases the photoactivity of the rutile by 15 times for the oxidation of acetone [8]. Furthermore, the activity increases with increasing Sn in $Sn_xTi_{1-x}O_2$ solid solution, and it peaks at a tin content of 0.075. The authors conclude that Sn substitution for Ti in TiO_2 lattice results in a decrease in the rate of photogenerated electron–hole recombination. This lower recombination is attributed to an increase in the band gap of the solid solution. They infer that the increase in the band gap with the Sn content in the $Sn_xTi_{1-x}O_2$ system is in large part due to an increase in its conduction band. In fact, our calculations predict, for all investigated compositions, that the increase in energy of the bottom of the conduction band is about 30% larger than the augment of the top of the valence band. When the system is illuminated by UV light of adequate wavelength, some electrons are promoted to the conduction band. Since the conduction band shifts toward higher potential, the energy of the electrons on the conduction band is enough to reduce oxygen in air. Thus, the photoexcited electrons and holes on the solid solution can be separated effectively and have a longer lifetime. Therefore, the increase in the photocatalytic oxidation–reduction potential of the semiconductor is inferred to be the origin of the enhanced photoactivity of $Sn_xTi_{1-x}O_2$ system. Our results reveal that this argument can be correct, since Fig. 2 shows that Fermi level of $Sn_xTi_{1-x}O_2$ solid solution increase with increasing x. However, theoretical results indicate that other effect can play a more important role as far as electron–hole recombination is concerned. Fig. 6 shows the band structure of $Sn_xTi_{1-x}O_2$ for $x = 1/12$ in the high-symmetry directions in the Brillouin zone, calculated with a $1 \times 2 \times 3$ supercell. This value of x has been selected as it approaches the optimum composition 0.075. It can be observed that the lowest

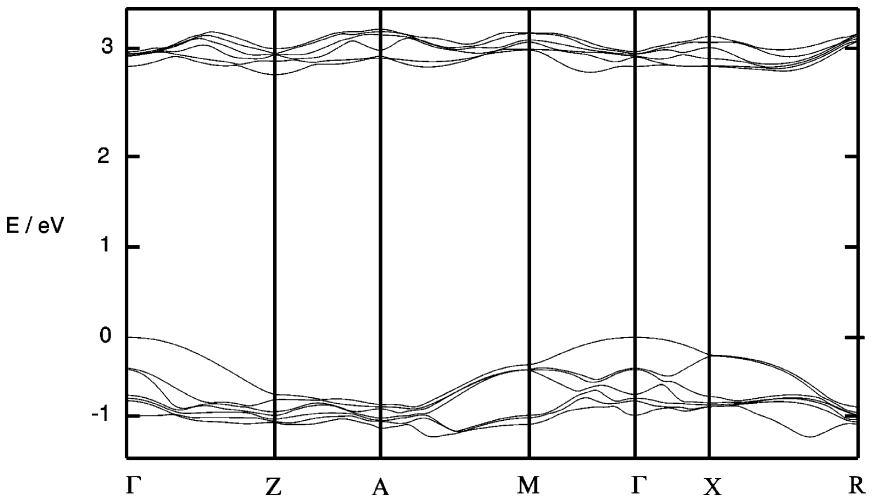

Fig. 6. Calculated energy-band structure for $Sn_xTi_{1-x}O_2$ system ($x = 1/12$). The energy scale is in eV and the origin of energy was arbitrarily set to be at the valence band maximum. The fractional coordinates of the high-symmetry points of de Brillouin zone used are: $\Gamma = 0, 0, 0$; $Z = 0, 0, 1/2$; $A = 1/2, 1/2, 1/2$; $M = 1/2, 1/2, 0$; $X = 0, 1/2, 0$; $R = 0, 1/2, 1/2$.

energy transition is forbidden, since it corresponds to an indirect band gap ($\Gamma \rightarrow Z$) of 2.9 eV. It is well known that an indirect band gap tends to inhibit the recombination of electrons and holes, since transitions from the bottom of the conduction band into the top of the valence band are forbidden [49]. Thus, in addition to increase in the oxidation–reduction potential of the oxide, Sn substitution for Ti in rutile TiO_2 prevents photogenerated electron–hole recombination by causing the lowest energy transition to be forbidden. These results account for the enhanced photoactivity of $Sn_xTi_{1-x}O_2$.

4. Conclusions

The electronic and geometrical structures of selected $Sn_xTi_{1-x}O_2$, $x = 0$–1, binary composition were investigated using periodic DFT calculations. The main results of the present study can be summarized as follows: (i) deviations from Vegard's law was found in the $Sn_xTi_{1-x}O_2$ system, (ii) band gap and Fermi level of $Sn_xTi_{1-x}O_2$ vary continuously from those of pure TiO_2 to those of pure SnO_2 with increasing x, and (iii) Sn substitution for Ti in rutile increases the oxidation–reduction potential of the oxide and renders the lowest energy transition to be indirect. These effects are believed to inhibit the photogenerated electron–hole recombination, and thus endow the enhanced photoactivity for $Sn_xTi_{1-x}O_2$ solid solutions.

Acknowledgements

The authors thank M.R. Cassia-Santos and P.R. Bueno for their helpful discussions. FRS thanks the Brazilian funding agency FAPESP for a postdoctoral grant. This study was also supported by the "Programa de Cooperación Internacional" maintained by CAPES (Brazil) and by the Ministerio de Educación y Cultura del Gobierno Español. The authors are indebted to Servei d'Informática of the Universitat Jaume I for providing us with excellent computer facilities.

References

[1] M. Radecka, K. Zakrzewska, M. Rekas, Sens. Actuators B 47 (1998) 194.
[2] K. Zakrzewska, Thin Solid Films 391 (2001) 229.
[3] K. Zakrzewska, M. Radecka, M. Rekas, Thin Solid Films 310 (1997) 161.
[4] M. Radecka, J. Przewoznik, K. Zakrzewska, Thin Solid Films 391 (2001) 247.

[5] W. Tai, J.-H. Oh, Sens. Actuators B 85 (2002) 154.
[6] V. Dusastre, D.E. Williams, J. Mater. Chem. 9 (1999) 445.
[7] P.R. Bueno, M.R. Cassia-Santos, L.G.P. Simões, J.W. Gomes, E. Longo, J. Am. Ceram. Soc. 85 (2002) 282.
[8] J. Lin, J.C. Yu, D. Lo, S.K. Lam, J. Catal. 183 (1999) 368.
[9] J. Yang, D. Li, X. Wang, X. Yang, L. Lu, J. Solid State Chem. 165 (2002) 193.
[10] P.A. Sermon, T.J. Walton, Solid State Ionics 101–103 (1997) 673.
[11] A.H. Schultz, V.S. Stubican, Philos. Mag. 18 (1968) 929.
[12] P.K. Gupta, A.R. Cooper, Philos. Mag. 21 (1970) 611.
[13] R.M. Cohen, D. Drobeck, A.V. Virkar, J. Am. Ceram. Soc. 71 (1988) C401.
[14] L.B. Kong, J. Ma, H. Huang, J. Alloys Compd. 336 (2002) 315.
[15] S. Begin-Colin, G. Le Caer, A. Mocellin, C. Jurenka, M. Zandona, J. Solid State Chem. 127 (1996) 98.
[16] F. Edelman, H. Hahn, S. Seifried, C. Alof, H. Hoche, A. Balogh, P. Werner, K. Zakrzewska, M. Radecka, P. Pasierb, A. Chack, V. Mikhelashvili, G. Eisenstein, Mater. Sci. Eng. B 69–70 (2000) 386.
[17] P.R. Bueno, E.R. Leite, L.O.S. Bulhões, E. Longo, C.O. Paiva-Santos, J. Eur. Ceram. Soc. 23 (2003) 887.
[18] T. Hirata, K. Ishioka, M. Kitajima, H. Doi, Phys. Rev. B 53 (1996) 8442.
[19] M. Park, T.E. Mitchell, A.H. Heuer, J. Am. Ceram. Soc. 58 (1975) 43.
[20] Y. Yamaguchi, Y. Nagasawa, K. Tabata, E. Suzuki, J. Phys. Chem. A 106 (2002) 411.
[21] J. Sauer, Chem. Rev. 89 (1989) 199.
[22] C.R.A. Catlow, G.D. Price, Nature 347 (1990) 243.
[23] C.R.A. Catlow, J.D. Gale, R.W. Grimes, J. Solid State Chem. 106 (1993) 13.
[24] M.L. Cohen, Int. J. Quant. Chem. 61 (1997) 603.
[25] P.J.D. Lindan, J. Muscat, S. Bates, N.M. Harrison, M. Gillan, Faraday Discuss. 106 (1997) 135.
[26] C. Pisani, J. Mol. Struct. (Theochem.) 463 (1999) 125.
[27] A. Groß, Theoretical Surface Science, Springer, Berlin, 2003.
[28] A. Fahmi, C. Minot, B. Silvi, M. Causà, Phys. Rev. B 47 (1993) 11717.
[29] M. Ramamoorthy, D. Vanderbilt, R.D. King-Smith, Phys. Rev. B 49 (1994) 16721.
[30] J. Muscat, V. Swamy, N.M. Harrison, Phys. Rev. B 65 (2002) 224112.
[31] M.P. Lara-Castells, J.L. Krause, Chem. Phys. Lett. 354 (2002) 483.
[32] M. Menetrey, A. Markovits, C. Minot, Surf. Sci. 524 (2003) 49.
[33] T.T. Rantala, T.S. Rantala, V. Lantto, Surf. Sci. 420 (1999) 103.
[34] M. Calatayud, J. Andrés, A. Beltrán, Surf. Sci. 430 (1999) 213.
[35] M. Melle-Franco, G. Pacchioni, Surf. Sci. 461 (2000) 54.
[36] J. Oviedo, M.J. Gillan, Surf. Sci. 463 (2000) 93.
[37] F.R. Sensato, R. Custódio, M. Calatayud, A. Beltrán, J. Andrés, J.R. Sambrano, E. Longo, Surf. Sci. 511 (2002) 408.
[38] M.W. Abee, D.F. Cox, Surf. Sci. 520 (2002) 65.
[39] V.R. Saunders, R. Dovesi, C. Roetti, M. Causà, N.M. Harrison, R. Orlando, C.M. Zicovich-Wilson, Crystal'98 User's Manual, University of Torino, Torino, 1998.
[40] A.D. Becke, J. Chem. Phys. 98 (1993) 5648.
[41] C. Lee, R.G. Yang, R.G. Parr, Phys. Rev. B 37 (1988) 785.
[42] C.-H. Hu, D.P. Chong, in: P. von Rague Schleyer (Ed.), Encyclopedia of Computational Chemistry, Wiley, Chichester, UK, 1998.
[43] J. Muscat, A. Wander, N.M. Harrison, Chem. Phys. Lett. 342 (2001) 397.
[44] A. Beltrán, J.R. Sambrano, M. Calatayud, F.R. Sensato, J. Andrés, Surf. Sci. 490 (2001) 116.
[45] P. Durand, J.C. Barthelat, Theoret. Chim. Acta 37 (1975) 283.
[46] B. Silvi, N. Fourati, R. Nada, C.R.A. Catlow, J. Phys. Chem. Solids 52 (1991) 1005.
[47] J.A. Nelder, R. Mead, Comput. J. (UK) 7 (1965) 308.
[48] A. Kokalj, J. Mol. Graph. Model. 17 (1999) 176.
[49] P.A. Cox, The Electronic Structure and Chemistry of Solids, Oxford University Press, Oxford, 1998.